ACS APPLIED MATERIALS & INTERFACES

Research Article

www.acsami.org

High-Performance Supercapacitor Electrode Based on the Unique ZnO@Co_3O_4 Core/Shell Heterostructures on Nickel Foam

Daoping Cai, Hui Huang, Dandan Wang, Bin Liu, Lingling Wang, Yuan Liu, Qiuhong Li,* and Taihong Wang*

Pen−Tung Sah Institute of Micro−Nano Science and Technology, Xiamen University, Xiamen 361000, People's Republic of China

Supporting Information

ABSTRACT: Currently, tremendous attention has been paid to the rational design and synthesis of unique core/shell heterostructures for high-performance supercapacitors. In this work, the unique ZnO@Co_3O_4 core/shell heterostructures on nickel foam are successfully synthesized through a facile and cost-effective hydrothermal method combined with a short post annealing treatment. Mesoporous Co_3O_4 nanowires are multidirectional growing on the rhombus-like ZnO nanorods. In addition, the growth mechanism for such unique core/shell heterostructures is also proposed. Supercapacitor electrodes based on the ZnO@Co_3O_4 and Co_3O_4 heterostructures on nickel foam are thoroughly characterized. The ZnO@Co_3O_4 electrode exhibits high capacitance of 1.72 F cm^{-2} (857.7 F g^{-1}) at a current density of 1 A g^{-1}, which is higher than that of the Co_3O_4 electrode. Impressively, the capacitance of the ZnO@Co_3O_4 electrode increases gradually from 1.29 to 1.66 F cm^{-2} (830.8 F g^{-1}) after 6000 cycles at a high current density of 6 A g^{-1}, indicating good long-term cycling stability. These results indicate the unique ZnO@Co_3O_4 electrode would be a promising electrode for high-performance supercapacitor applications.

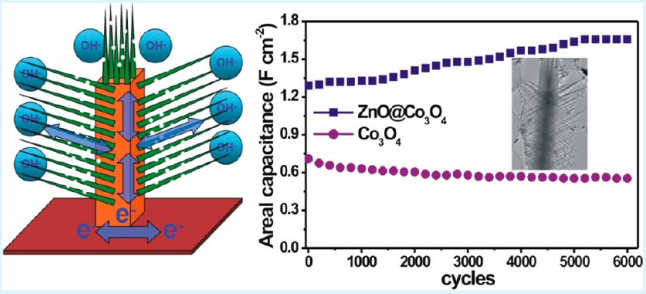

KEYWORDS: *cobalt oxides, core/shell, electrode material, binder-free, supercapacitor*

1. INTRODUCTION

Supercapacitors, also called electrochemical capacitors, have attracted great research interest from both industry and academia because they are specified to be as important as batteries for future energy storage systems by the U.S. Department of Energy.[1,2] Among the various energy storage devices, supercapacitors are superior in the fields of fast charge/discharge process, high power density, long lifespan, safety and environmental friendliness.[3−5] Although carbon-based materials have been widely investigated as electrode materials, the fairly low specific and volumetric capacitances have badly hindered their further practical use for high-performance supercapacitors.[6,7] Recently, extensive attention has been paid to investigate pseudocapacitive transition metal oxides (such as RuO_2,[8,9] MnO_2,[10] NiO,[11] Co_3O_4,[12−15] etc.), which can obtain a much higher specific capacitance and energy density because they can supply different oxidation states for efficient redox reactions. Among them, Co_3O_4 is particularly attractive as high-performance electrode materials owing to its high theoretical capacitance (ca. 3560 F g^{-1}), as well as low cost, abundant resources and environmental friendliness. For example, Rao et al. have synthesized the ultralayered Co_3O_4 structures, which exhibited high specific capacitance of 548 F g^{-1} at a current density of 8 A g^{-1}, as well as excellent cycling stability.[14] Tu et al. reported the hydrothermal synthesis of freestanding Co_3O_4 nanowire arrays grown on nickel foam, which delivered a high capacitance of 754 F g^{-1} at 2 A g^{-1}.[15]

Currently, tremendous attention has been paid to the rational design and synthesis of unique core/shell heterostructures to achieve enhanced electrochemical, optical, electrical and mechanical properties.[16−19] Zinc oxide (ZnO), as one of the most attractive multifunctional materials, is extensively studied in piezotronics and electronics devices, surface switches, strain sensors and photocatalysis due to its good electric conduction and special optoelectronic properties, as well as the excellent chemical and thermal stabilities.[20,21] Among various core/shell heterostructures, ZnO is usually selected as the ideal core material that can function as a strong mechanical support and electron transport pathway due to its good chemical stability and high electrical conductivity.[22−26] Recently, Sun and co-workers demonstrated the electrodeposition of Ni_3S_2 and $Ni(OH)_2$ on a ZnO array supported on Ni foam. The as-synthesized ZnO@Ni_3S_2 and ZnO@$Ni(OH)_2$ electrodes exhibited excellent electrochemical performance when evaluated as binder-free electrodes for supercapacitors.[24,25] Li et al. reported ZnO@MoO_3 core/shell nanocables, which exhibited much enhanced specific capacitance than that of MoO_3 nanoparticles.[26] However, the fabrication of well-defined core/shell heterostructures via facile and simple methods still remains a big challenge. In addition, most of the present reports about synthesis of ZnO core/shell

Received: June 4, 2014
Accepted: August 25, 2014
Published: August 25, 2014

heterostructures are via two-step methods, that is, by electrodeposition of shell materials on the preformed ZnO cores,[24−26] which could be time-consuming and costly. Therefore, it is significant to develop a simple and cost-effective method to synthesize well-defined ZnO core/shell heterostructures.

In this work, we successfully synthesize the unique ZnO@Co_3O_4 core/shell heterostructures on nickel foam through a facile and cost-effective hydrothermal method combined with a short post annealing treatment. The unique ZnO@Co_3O_4 core/shell heterostructures are directly grown on nickel foam with good mechanical adhesion and electrical contact. Directly grown electrode materials on a current collector not only simplify the electrode processing but also avoid the use of polymer binder and conducting additives, allowing for more effectively charge and mass exchange.[27−29] 3D nickel foam with uniform macropores, large supporting area and high electrical conductivity is selected as the current collector.[17] As a binder-free electrode for supercapacitors, the unique ZnO@Co_3O_4 electrode exhibits excellent electrochemical performance.

2. EXPERIMENTAL DETAILS

2.1. Materials Preparation. All of the reagents were of analytical purity grade and used without further purification. Before the synthesis, the Ni foam substrate (2 × 1 × 0.1 cm) was washed by sonication in acetone, ethanol and deionized (DI) water for 10 min, respectively. Typically, 2 mmol $Co(NO_3)_2{\cdot}6H_2O$, 1 mmol $Zn(NO_3)_2{\cdot}6H_2O$ and 4 mmol NH_4F were dissolved in 30 mL of deionized (DI) water to form a homogeneous solution. Subsequently, 8 mmol of urea was added into the above homogeneous solution with magnetic stirring and then transferred to a 50 mL Teflon-lined stainless steel autoclave. The cleaned Ni foam substrate was immersed into the reaction solution. After that, the autoclave was heated to 120 °C for 5 h and then cooled down to room temperature naturally. The Ni foam loaded with precursor was washed with distilled water and dried in the oven. The final product was obtained by annealing the precursor at 400 °C for 3 h in air. The Co_3O_4 heterostructures on nickel foam was synthesized at the same condition except for no addition of the $Zn(NO_3)_2{\cdot}6H_2O$. The mass loadings of the ZnO@Co_3O_4 and Co_3O_4 heterostructures on nickel foam were around 2.0 and 1.5 mg cm^{-2}, respectively.

2.2. Materials Characterization. The morphology and microstructure of the products were observed using scanning electron microscopy (SEM, Zeiss Supra 55) and transmission electron microscopy (TEM, JEM-2100). The crystal structure and phase purity of the products were characterized by X-ray diffraction (XRD, Rigaku Ultima IV) with Cu Kα irradiation.

2.3. Electrochemical Measurements. The electrochemical measurements were carried out using a CHI660E electrochemical workstation at room temperature in a three-electrode electrochemical cell. The ZnO@Co_3O_4 and Co_3O_4 heterostructures on nickel foam (1 cm^2 in area) were directly investigated as the working electrodes. The reference electrode was a standard calomel electrode (SCE), and the counter electrode was a Pt foil. A 2 M KOH aqueous solution was used as the electrolyte. Electrochemical impedance spectroscopy (EIS) measurements were measured in the frequency range from 0.01 Hz to 100 kHz. The specific capacitance (C) was calculated from the following formulas:[27]

$$C = \frac{It}{SV} \quad \text{and} \quad C = \frac{It}{mV} \tag{1}$$

where I (A), t (s), V (V), S (cm^2) and m (g) represent the discharge current, discharge time, potential window, area of the working electrode and the mass of electrode materials, respectively.

3. RESULT AND DISCUSSION

3.1. Synthesis and Structural Analysis. The morphologies of the ZnO@Co_3O_4 core/shell heterostructures on nickel foam were first investigated by SEM. Figure 1 shows the SEM images of the ZnO@Co_3O_4 core/shell heterostructures on Ni foam at different magnifications. It can be observed that the nickel foam is uniformly covered by the ZnO@Co_3O_4 heterostructures on a large scale (Figure 1a,b). The ZnO@Co_3O_4 heterostructures display bundle-like nanostructure, as observed from the high magnification SEM image (Figure 1c−e). The Co_3O_4 nanowires with diameters of 50−80 nm are grown on the ZnO core and self-assembled forming clusters (Figure 1f). TEM studies provide further insight into the unique ZnO@Co_3O_4 core/shell heterostructures. As shown in Figure 2a,b, the core/shell structure is easily distinguished from the TEM image from an individual ZnO@Co_3O_4 core/shell heterostructure, where the ZnO core is fully covered by the Co_3O_4 nanowires. The energy dispersive spectrometry (EDS) analysis reveals that signal of Zn is strong in the core region (A1), whereas quite weak in the shell region (A2) (Figure S1, Supporting Information). In addition, the mapping analysis further indicates this unique core/shell structure, as shown in Figure 3a. These Co_3O_4 nanowires are highly porous, made up of numerous nanocrystallites about 10−20 nm in size (Figure 2c,d). It is thought that these mesopores are due to the release of gases during the thermal treatment. It is well accepted that the mesoporous structures can facilitate the transport of the

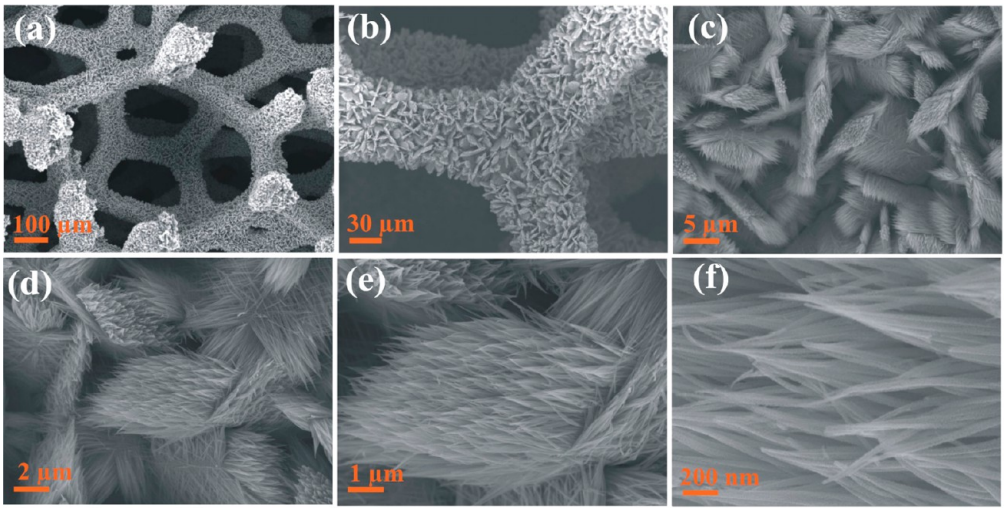

Figure 1. (a−f) Typical SEM images of the ZnO@Co_3O_4 core/shell heterostructures on nickel foam at different magnifications.

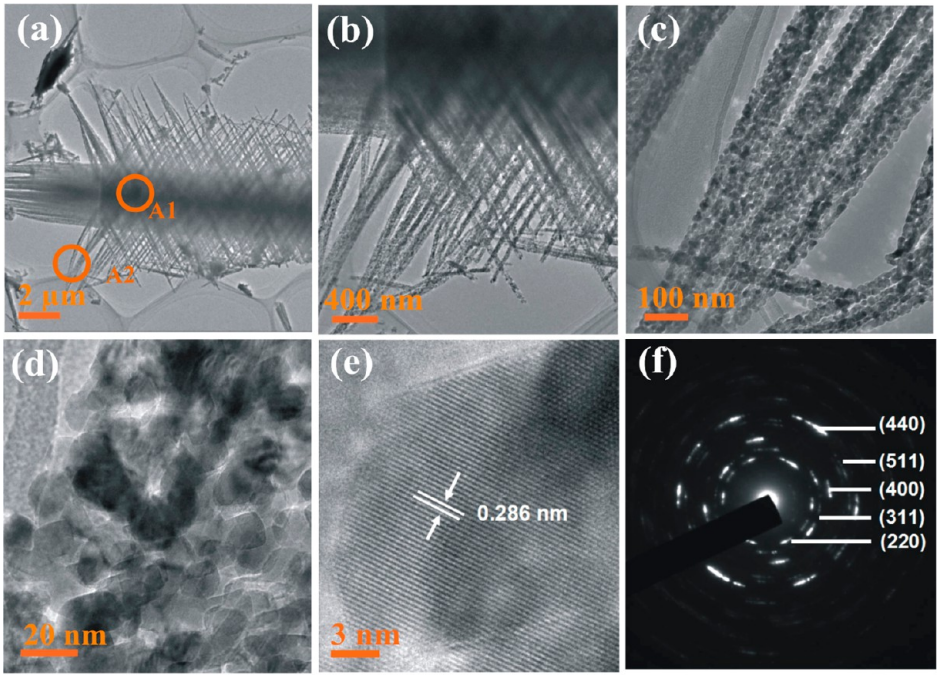

Figure 2. (a) Low and (b) high magnification TEM images of an individual ZnO@Co_3O_4 heterostructure; (c) low and (d) high magnification TEM images, (e) high-resolution TEM image and (f) the corresponding SAED pattern of the Co_3O_4 nanowires.

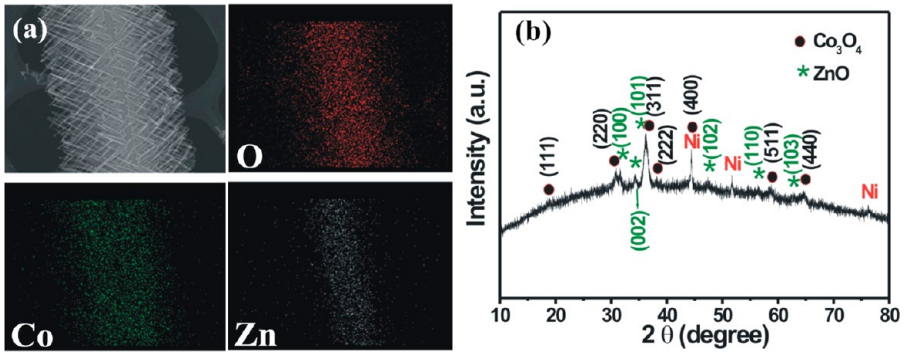

Figure 3. (a) Mapping analysis and (b) XRD pattern of the ZnO@Co_3O_4 core/shell heterostructures scratched from nickel foam.

electrolyte and ensure efficient contact between the active material and the electrolyte when used as a supercapacitor electrode.[30,31] The HRTEM image of the Co_3O_4 nanowires shows an interplanar spacing of 0.286 nm, corresponding to the (220) plane of the Co_3O_4 (JCPDS No. 42-1467), as shown in Figure 2e.[12,13,15] The corresponding selected area electron diffraction (SAED) pattern reveals the polycrystalline nature of the mesoporous Co_3O_4 nanowires, and the diffraction rings are readily indexed to the (220), (311), (400), (511) and (440) planes of the Co_3O_4 crystal structure (JCPDS No. 42-1467).[12,13,15] In addition, the ZnO@Co_3O_4 (10 min) sample was also investigated by TEM. The TEM and HRTEM images and SAED pattern of ZnO@Co_3O_4 (10 min) are shown in Figure S2 (Supporting Information). The spacing of the lattice fringes is calculated to be 0.260 nm, which can be indexed to the (002) planes of the hexagonal ZnO. And the diffraction rings in the SAED pattern can be readily indexed to the (002), (101), (102), (110), (103) and (112) planes of the hexagonal ZnO (JCPDS No. 36-1451).[26]

To further investigate the crystal structure and phase composition, the ZnO@Co_3O_4 core/shell heterostructures were scratched from nickel foam for XRD analysis, as shown in Figure 3. Besides the three peaks from the nickel foam substrate, the other diffraction peaks can be indexed to the (111), (220), (311), (222), (400), (511) and (440) planes of the cubic Co_3O_4 (JCPDS No. 42-1467)[12,13,15] and the (100), (002), (101), (102), (110) and (103) planes of the hexagonal ZnO (JCPDS No. 36-1451),[26] which is consistent with the TEM analysis. The EDS analysis indicates that there exists some weak Zn signal in the Co_3O_4 shell region, which is attributed to the partial substitution of some Co ions by Zn ions. It is worth noting that the replacement of Co ions with Zn ions only slightly changes the lattice parameters while the crystal structure is maintained.

To investigate the growth mechanism for such unique ZnO@Co_3O_4 core/shell heterostructures, a series of experiments with different hydrothermal reaction times are performed. Figure 4 shows the SEM images of the products obtained at different reaction times after annealing treatment. At the beginning of the hydrothermal reactions, Co^{2+} and Zn^{2+} ions can interact with F^- ions to form CoF^+ and ZnF^+ complexes in the homogeneous solution.[32−36] When the reaction temperature increases to 120 °C, urea can provide OH^- and carbonate ions simultaneously during the hydrolysis. Due to the lower solubility product (K_{sp}) value of $Zn(OH)_2$ than that of $Co(OH)_2$, ZnF^+ ions and OH^- ions can

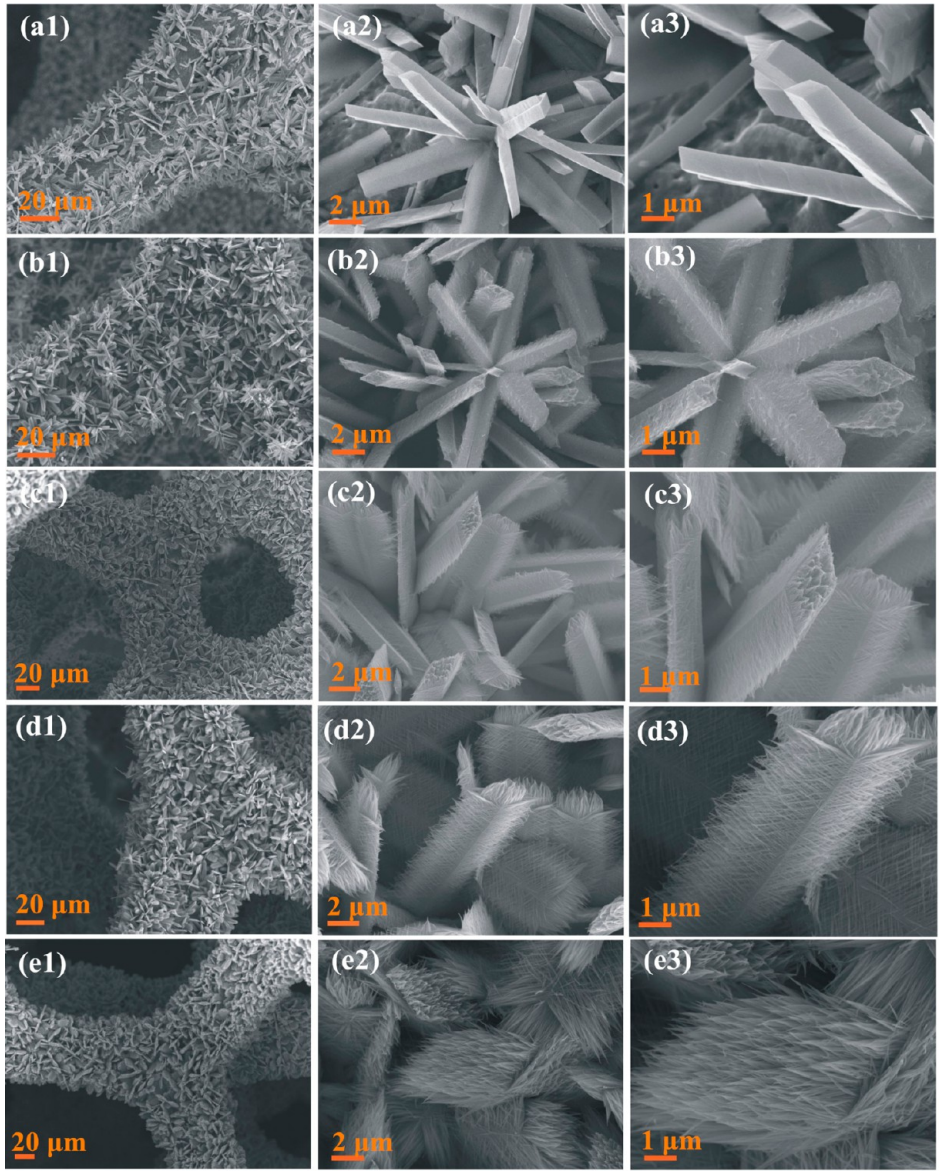

Figure 4. Low and high magnification SEM images of the products obtained at different reaction times after annealing treatment: (a1−a3) 10 min, (b1−b3) 30 min, (c1−c3) 1 h, (d1−d3) 2 h and (e1−e3) 5 h.

easily combine into Zn(OH)F precipitate and firmly grow onto the substrate through the functional groups (e.g., hydroxyl groups) on the surface of nickel foam.[33] 3D flower-like nanoarchitectures made up of many rhombus-like ZnO nanorods are observed on the nickel foam (Figure 4a1−a3). When the ZnF^+ ions are consumed to some degree, the CoF^+ ions begin to precipitate into nanoparticles on the rhombus-like Zn(OH)F nanorods. It is worth noting that carbonate anions can replace F^- due to its strong affinity to Co^{2+} to produce needle-like cobalt hydroxide carbonate.[36] Figure 4b1−b3 shows that the surface of the rhombus-like ZnO nanorods becomes rough and covered by a thin film of small nanoparticles. The XRD pattern of the product (obtained at 30 min) scratched from nickel foam is shown in Figure S3 (Supporting Information), where the strong diffraction peaks from ZnO phase are observed. When the reaction time is prolonged, the cobalt hydroxide carbonate nanowires gradually grow longer (Figure 4d1−d3). Finally, the self-assembled $ZnO@Co_3O_4$ core/shell heterostructures on nickel foam are obtained after a short post annealing treatment (Figure 4e1−e3).

The related chemical reactions occurred during the hydrothermal synthesis could be expressed using the following formulas:[35−37]

$$CO(NH_2)_2 + H_2O \rightarrow 2NH_3 + CO_2$$

$$H_2O + NH_3 \rightarrow OH^- + NH^{4+}$$

$$ZnF^+ + OH^- \rightarrow Zn(OH)F$$

$$CO_2 + H_2O \rightarrow CO_3^{2-} + 2H^+$$

$$CoF^+ + xOH^- + 0.5(2-x)CO_3^{2-} + nH_2O \rightarrow Co(OH)_x(CO_3)_{0.5(2-x)} \bullet nH_2O + F^-$$

$$Zn(OH)F \rightarrow ZnO + HF\uparrow$$

$$Co(OH)_x(CO_3)_{0.5(2-x)} \bullet nH2O + O_2 \rightarrow Co_3O_4 + CO_2 \uparrow + H_2O\uparrow$$

dx.doi.org/10.1021/am5035494 | ACS Appl. Mater. Interfaces 2014, 6, 15905−15912

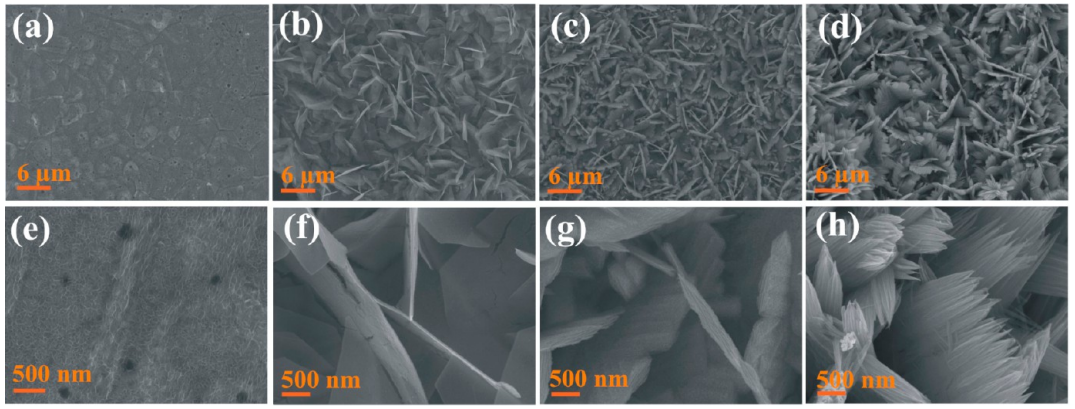

Figure 5. Low and high magnification SEM images of the products (without the addition of $Zn(NO_3)_2$ obtained at different reaction times after annealing treatment: (a and e) 10 min, (b and f) 30 min, (c and g) 1 h and (d and h) 2 h.

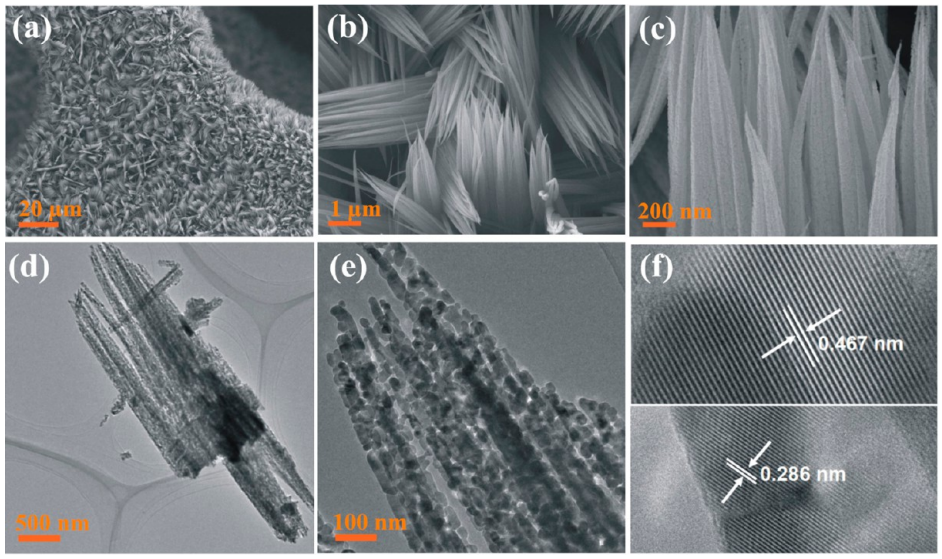

Figure 6. (a–c) Typical SEM images of the Co_3O_4 heterostructures (5 h) on nickel foam at different magnifications; (d) low and (e) high magnification TEM images and (f) high-resolution TEM images of the Co_3O_4 heterostructure.

On the basis of the above results, the unique ZnO@Co_3O_4 core/shell heterostructure is formed by the subsequent multidirectional growing of Co_3O_4 nanowires on the rhombus-like ZnO nanorods. Without the addition of $Zn(NO_3)_2$, the SEM images of the products obtained at different reaction times after annealing treatment are also investigated, as shown in Figure 5. The growth mechanism of the products in the absence of $Zn(NO_3)_2$ is different from that of ZnO@Co_3O_4 core/shell heterostructures. At the early stage of reaction, numerous nanoparticles nucleated on the surface of the Ni foam, forming an uneven layer (Figure 5a,e). The nanoparticles then grow into small nanosheets and then quickly become large (Figure 5b,f). As the reaction proceeded, these nanosheets became thicker with a rough surface (Figure 5c,g). Subsequently, these nanosheets act as the backbone for the cobalt hydroxide carbonate nanowires to grow on (Figure 5d,h). By further increasing the reaction time to 5 h, the cobalt hydroxide carbonate nanowires become long and dense (Figure 6a–c). Finally, the Co_3O_4 nanosheet–nanowire heterostructures on nickel foam are obtained after thermal annealing. The growth process of the Co_3O_4 heterostructures is quite similar to the hierarchical Co_3O_4 nanosheet@nanowire arrays and self-assembled $NiCo_2O_4$ heterostructure arrays.[13,38]

Figure 6a–c shows the SEM images of the Co_3O_4 heterostructures grown on Ni foam at different magnifications. It can be seen that the nickel foam is uniformly covered by the Co_3O_4 heterostructures. The high magnification SEM image reveals the highly porous feature of the Co_3O_4 nanowires. The XRD pattern of the Co_3O_4 heterostructures scratched from nickel foam is shown in Figure S3 (Supporting Information). All the diffraction peaks can be assigned to the (111), (220), (311), (222), (400), (511) and (440) planes of the cubic Co_3O_4 (JCPDS No. 42-1467).[12,13,15] Figure 6d,e shows the low and high magnification TEM images of the Co_3O_4 nanowires, further indicating the mesoporous characteristic. The lattice fringes of 0.467 and 0.286 nm can correspond to the (111) and (220) crystal planes of cubic phase Co_3O_4, respectively, as seen in the HRTEM image (Figure 6f).

3.2. Electrochemical Analysis. The obtained ZnO@Co_3O_4 and Co_3O_4 heterostructures on nickel foam were directly evaluated as binder-free electrodes for supercapacitors. The electrochemical measurements were carried out in a three-electrode electrochemical cell where a 2 M KOH aqueous solution is used as the electrolyte. Figure 7a,b shows the cyclic voltammogram (CV) curves of the ZnO@Co_3O_4 and Co_3O_4 electrodes recorded at various scan rates within the potential

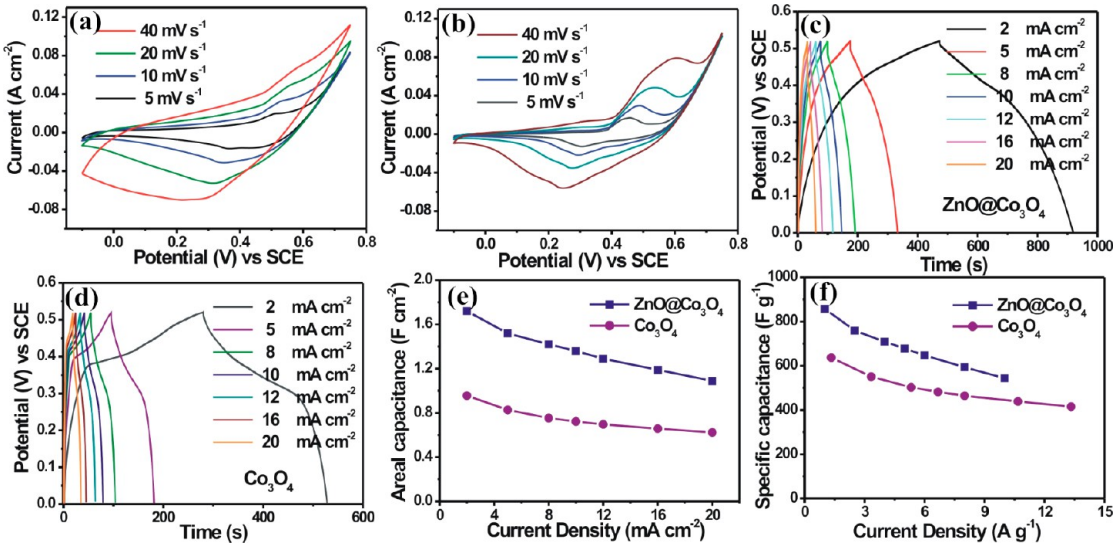

Figure 7. CV curves of the (a) $ZnO@Co_3O_4$ and (b) Co_3O_4 electrodes at different scan rates; charge and discharge curves of the (c) $ZnO@Co_3O_4$ and (d) Co_3O_4 electrodes at different current densities; (e and f) the calculated areal and specific capacitance as a function of the current density.

range of −0.1 to +0.75 V. A pair of redox peaks can be observed in all the CV curves, which indicates the electrochemical performance of electrodes is resulted from the pseudocapacitive capacitance.[14,27,31] The shape of the CV curves is evidently different from the CV curves of EDLCs that are similar to an ideal rectangular shape. With increasing scan rates, the positions of anodic peaks shift to a more anodic direction, which could be attributed to the internal resistance of the electrode. Figure S4 (Supporting Information) shows the CV comparison of the two electrodes recorded at a scan rate of 10 mV s^{-1}. The CV curve integral area of the $ZnO@Co_3O_4$ electrode is much larger than of Co_3O_4 electrode, indicating that larger capacitance of the $ZnO@Co_3O_4$ electrode is obtained. It is noting that the area of the CV curve of Ni foam substrate is very small, which suggests that the capacitance contribution from nickel foam can be negligible.

The typical charge and discharge curves of the two electrodes at different current densities within the potential window of 0−0.52 V are shown in Figure 7c,d. The areal and specific capacitance for the $ZnO@Co_3O_4$ and Co_3O_4 electrodes can be calculated on the basis of the charge and discharge curves, and the results are presented in Figure 7e,f. The $ZnO@Co_3O_4$ electrode exhibits high areal capacitance values of 1.72, 1.52, 1.42, 1.36, 1.29, 1.19 and 1.09 F cm^{-2}, and specific capacitance values of 857.7, 759.6, 709.2, 677.9, 647.3, 593.8 and 544.2 F g^{-1} at different current densities of 2, 5, 8, 10, 12, 16 and 20 mA cm^{-2}, respectively. The capacitance can retain 63.4% of its initial value as the current density increases by 10 times, indicating a good rate capability. For comparison, the Co_3O_4 electrode exhibits lower areal capacitance values of 956, 827, 754, 723, 697, 658 and 623 mF cm^{-2}, and specific capacitance values of 637.2, 551.3, 502.6, 482.1, 464.6, 439.0 and 415.4 F g^{-1} at the same current densities. The capacitance of the $ZnO@Co_3O_4$ electrode is also superior to previously binder-free electrodes reported elsewhere, such as Co_3O_4/NiO core/shell nanowire arrays (452 F g^{-1} at 2 A g^{-1}),[16] $NiCo_2O_4$ nanoneedle arrays on nickel foam (0.99 F cm^{-2} at 5.56 mA cm^{-2})[27] and $CoMoO_4$ nanoplate arrays on nickel foam (1.15 F cm^{-2} at 8 mA cm^{-2}).[39]

The long-term cycling stability of electrodes is also important requirement for practical supercapacitor applications, which was investigated by the repeated charge and discharge measurement at a high current density of 6 A g^{-1} for 6000 cycles, as shown in Figure 8. For the Co_3O_4 electrode, the areal capacitance is 710 mF cm^{-2} in the first cycle, and it gradually decreases to 554 mF cm^{-2} after 6000 cycles, leading to an overall capacitance loss of ∼22.0%. Interestingly, the areal capacitance of the $ZnO@Co_3O_4$ electrode gradually increases and keeps at a high capacitance of 1.66 F cm^{-2} (830.8 F g^{-1}) after 6000 cycles, which is generally explained by the activation of the electrode. The possible explanation is that only a part of electrode material is active at first. As the electrolyte gradually penetrates into the inner region of the electrode, more and more sites become activated and contribute to the increase of capacitance.[16,38] The SEM images of the $ZnO@Co_3O_4$ core/shell heterostructures on nickel foam after 6000 cycles is shown in Figure S5 (Supporting Information), the $ZnO@Co_3O_4$ core/shell heterostructures are well maintained with little structural deformation.

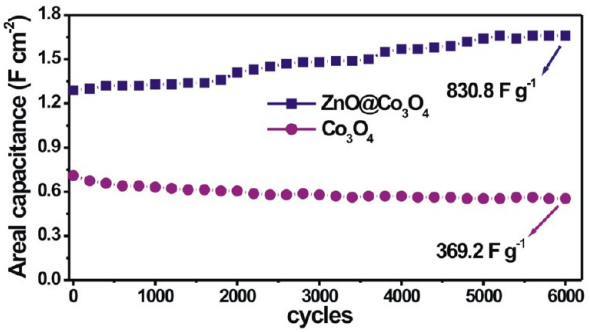

Figure 8. Cycling performance of the $ZnO@Co_3O_4$ and Co_3O_4 electrodes at a high current density of 6 A g^{-1} for 6000 cycles.

The EIS measurements were further carried out to investigate the electrochemical behavior of the $ZnO@Co_3O_4$ electrode before and after cycling. The corresponding Nyquist plots obtained in the frequency range from 0.01 to 100 kHz at open circuit potential are shown in Figure 9a. The impedance spectra are composed of a semicircle at high frequency region and a spike at low frequency region. The intercept of the curve at Z′-axis at the high frequency represents the resistance of the electrochemical system (R_s, which includes the intrinsic resistance of the substrate, ionic resistance of electrolyte and contact resistance between current collector and active material) and the semicircle

dx.doi.org/10.1021/am5035494 | ACS Appl. Mater. Interfaces 2014, 6, 15905−15912

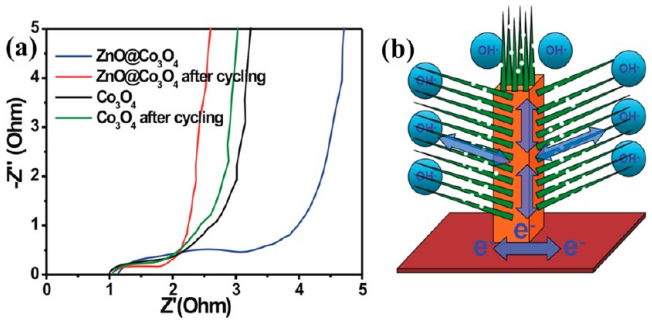

Figure 9. (a) Impedance Nyquist plots of the ZnO@Co_3O_4 and Co_3O_4 electrode before and after cycling; (b) schematic diagram showing the advantages of the ZnO@Co_3O_4 electrode for supercapacitors.

diameter represents the charge-transfer resistance (R_{ct}).[17,40,41] It can be seen that both R_s and R_{ct} of the ZnO@Co_3O_4 electrode become lower after a long-term cycling test. The R_s and R_{ct} of the ZnO@Co_3O_4 electrode, after cycling, is superior to the Co_3O_4 nanowires directly grown the nickle foam, indicating the fast electron transport through ZnO nanorods to the current collector. The EIS results imply the enhanced utilization of the electrode materials and the easy penetration of the electrolyte within the electrode, which can well explain the increase of the capacitance as described above.

As shown in Figure 9b, the excellent performance of the ZnO@Co_3O_4 electrode could be attributed to the following aspects: (1) due to the good chemical stability of ZnO, the rhombus-like ZnO nanorods can act as stable scaffolds and provide numerous sites for Co_3O_4 nanowire growth;[20,21] (2) the ZnO nanorods bridge the Co_3O_4 nanowires with the current collector, which can facilitate electron transport during the processes of charging and discharging because of its high electrical conductivity;[23−25] (3) the mesoporous structures for the Co_3O_4 nanowires can facilitate the transport of the electrolyte and ensure efficient contact between the electrode material and the electrolyte, thus enhancing the electrochemical kinetics;[30,31] (4) the ZnO@Co_3O_4 core/shell heterostructures are directly grown on the current collector, which can ensure strong mechanical adhesion and good electrical contact with the conductive substrate. Moreover, this electrode design can avoid the use of a polymer binder and conducting additives, resulting in high capacitance even at high current densities by improving the utilization of the electrode material.[27−29]

CONCLUSION

In this work, we demonstrate a facile and cost-effective hydrothermal method to synthesize the unique ZnO@Co_3O_4 core/shell heterostructures on nickel foam for the first time. In addition, a series of experiments are also performed to investigate the growth mechanism. It is found that the unique ZnO@Co_3O_4 core/shell heterostructure is formed by the subsequent multidirectional growing of Co_3O_4 nanowires on the rhombus-like ZnO nanorod. Without the addition of $Zn(NO_3)_2$, the Co_3O_4 heterostructures on nickel foam are obtained instead. The as-synthesized ZnO@Co_3O_4 and Co_3O_4 heterostructures on nickel foam are directly evaluated as binder-free electrodes for supercapacitors. The electrochemial results show that the ZnO@Co_3O_4 electrode exhibits high capacitance of 1.72 F cm^{-2} (857.7 F g^{-1}) at a current density of 2 mA cm^{-2}, which is superior to that of the Co_3O_4 electrode. Impressively, the ZnO@Co_3O_4 electrode also exhibits good long-term cycling stability. The capacitance of the ZnO@Co_3O_4 electrode increases gradually from 1.29 to 1.66 F cm^{-2} (830.8 F g^{-1}) after 6000 cycles at a high current density of 6 A g^{-1}. These results indicate the unique ZnO@Co_3O_4 electrode would be a promising electrode for supercapacitor applications. It is also thought that the unique ZnO@Co_3O_4 core/shell heterostructures would hold potential applications in other fields, such as chemical and electrochemical sensing, solar cells, catalysis and field emission.

ASSOCIATED CONTENT

Supporting Information

EDS characterizations for the ZnO@Co_3O_4 core/shell heterostructure, TEM observations of the ZnO@Co_3O_4 sample (obtained at 10 min), XRD patterns of the product (obtained at 30 min) and Co_3O_4 heterostructures, CV comparison of the two electrodes recorded at a scan rate of 10 mV s^{-1} and SEM images of the ZnO@Co_3O_4 core/shell heterostructures on nickel foam after 6000 cycles. This material is available free of charge via the Internet at http://pubs.acs.org.

AUTHOR INFORMATION

Corresponding Authors

*Taihong Wang. E-mail: thwang@xmu.edu.cn. Tel.: +86-0592-2183063. Fax: +86-0592-2197196.

*Qiuhong Li. E-mail: liqiuhong2004@hotmail.com. Tel.: +86-0592-2183063. Fax: +86-0592-2197196.

Notes

The authors declare no competing financial interest.

ACKNOWLEDGMENTS

This research was partly supported by the National Basic Research Program of China (Grant No. 2007CB310500) and the National Natural Science Foundation of China (Grant No. 61376073).

REFERENCES

(1) Simon, P.; Gogotsi, Y. Materials for Electrochemical Capacitors. *Nat. Mater.* **2008**, *7*, 845−854.

(2) Wang, G.; Zhang, L.; Zhang, J. A Review of Electrode Materials for Electrochemical Supercapacitors. *Chem. Soc. Rev.* **2012**, *41*, 797−828.

(3) Liu, C.; Li, F.; Ma, L. P.; Cheng, H. M. Advanced Materials for Energy Storage. *Adv. Mater.* **2010**, *22*, E28−E62.

(4) Zhang, Q.; Uchaker, E.; Candelaria, S. L.; Cao, G. Nanomaterials for Energy Conversion and Storage. *Chem. Soc. Rev.* **2013**, *42*, 3127−3171.

(5) Zhao, X.; Sanchez, B. M.; Dobson, P. J.; Grant, P. S. The Role of Nanomaterials in Redox-based Supercapacitors for Next Generation Energy Storage Devices. *Nanoscale* **2011**, *3*, 839−855.

(6) Huang, Y.; Liang, J.; Chen, Y. An Overview of the Applications of Graphene-based Materials in Supercapacitors. *Small* **2012**, *8*, 1805−1834.

(7) Zhang, L. L.; Zhao, X. S. Carbon-based Materials as Supercapacitor Electrodes. *Chem. Soc. Rev.* **2009**, *38*, 2520−2531.

(8) Wu, X.; Zeng, Y.; Gao, H.; Su, J.; Liu, J.; Zhu, Z. Template Synthesis of Hollow Fusiform $RuO_2 \cdot xH_2O$ Nanostructure and Its Supercapacitor Performance. *J. Mater. Chem. A* **2013**, *1*, 469−472.

(9) Hu, C. C.; Chang, K. H.; Lin, M. C.; Wu, Y. T. Design and Tailoring of the Nanotubular Arrayed Architecture of Hydrous RuO_2 for Next Generation Supercapacitors. *Nano Lett.* **2006**, *6*, 2690−2695.

(10) Wei, W.; Cui, X.; Chen, W.; Ivey, D. G. Manganese Oxide-based Materials as Electrochemical Supercapacitor Electrodes. *Chem. Soc. Rev.* **2011**, *40*, 1697−1721.

(11) Yuan, C.; Zhang, X.; Su, L.; Gao, B.; Shen, L. Facile Synthesis and Self-Assembly of Hierarchical Porous NiO Nano/Micro Spherical

Superstructures for High Performance Supercapacitors. *J. Mater. Chem.* **2009**, *19*, 5772−5777.
(12) Zhu, T.; Chen, J. S.; Lou, X. W. Shape-Controlled Synthesis of Porous Co_3O_4 Nanostructures for Application in Supercapacitors. *J. Mater. Chem.* **2010**, *20*, 7015−7020.
(13) Yang, Q.; Lu, Z.; Chang, Z.; Zhu, W.; Sun, J.; Liu, J.; Sun, X.; Duan, X. Hierarchical Co_3O_4 Nanosheet@nanowire Arrays with Enhanced Pseudocapacitive Performance. *RSC Adv.* **2012**, *2*, 1663−1668.
(14) Meher, S. K.; Rao, G. R. Ultralayered Co_3O_4 for High-Performance Supercapacitor Applications. *J. Phys. Chem. C* **2011**, *115*, 15646−15654.
(15) Xia, X. H.; Tu, J. P.; Zhang, Y. Q.; Mai, Y. J.; Wang, X. L.; Gu, C. D.; Zhao, X. B. Freestanding Co_3O_4 Nanowire Array for High Performance Supercapacitors. *RSC Adv.* **2012**, *2*, 1835−1841.
(16) Xia, X.; Tu, J.; Zhang, Y.; Wang, X.; Gu, C.; Zhao, X.; Fan, H. J. High-Quality Metal Oxide Core/Shell Nanowire Arrays on Conductive Substrates for Electrochemical Energy Storage. *ACS Nano* **2012**, *6*, 5531−5538.
(17) Zhou, C.; Zhang, Y.; Li, Y.; Liu, J. Construction of High-Capacitance 3D CoO@Polypyrrole Nanowire Array Electrode for Aqueous Asymmetric Supercapacitor. *Nano Lett.* **2013**, *13*, 2078−2085.
(18) Xue, X. Y.; Chen, Z. H.; Xing, L. L.; Yuan, S.; Chen, Y. J. SnO_2/α-MoO_3 Core-Shell Nanobelts and Their Extraordinarily High Reversible Capacity as Lithium-Ion Battery Anodes. *Chem. Commun.* **2011**, *47*, 5205−5207.
(19) Zhang, N.; Liu, S.; Xu, Y. J. Recent Progress on Metal Core@Semiconductor Shell Nanocomposites as a Promising Type of Photocatalyst. *Nanoscale* **2012**, *4*, 2227−2238.
(20) Yang, P.; Xiao, X.; Li, Y.; Ding, Y.; Qiang, P.; Tan, X.; Mai, W.; Lin, Z.; Wu, W.; Li, T.; Jin, H.; Liu, P.; Zhou, J.; Wong, C. P.; Wang, Z. L. Hydrogenated ZnO Core-Shell Nanocables for Flexible Supercapacitors and Self-Powered Systems. *ACS Nano* **2013**, *7*, 2617−2626.
(21) Wang, Z.; Zhu, Z.; Qiu, J.; Yang, S. High Performance Flexible Solid-State Asymmetric Supercapacitors from MnO_2/ZnO Core−Shell Nanorods//Specially Reduced Graphene Oxide. *J. Mater. Chem. C* **2014**, *2*, 1331−1336.
(22) Sun, X.; Li, Q.; Lu, Y.; Mao, Y. Three-Dimensional ZnO@MnO_2 Core@Shell Nanostructures for Electrochemical Energy Storage. *Chem. Commun.* **2013**, *49*, 4456−4458.
(23) Liu, J.; Cheng, C.; Zhou, W.; Li, H.; Fan, H. J. Ultrathin Nickel Hydroxidenitrate Nanoflakes Branched on Nanowire Arrays for High-Rate Pseudocapacitive Energy Storage. *Chem. Commun.* **2011**, *47*, 3436−3438.
(24) Xing, Z.; Chu, Q.; Ren, X.; Ge, C.; Qusti, A. H.; Asiri, A. M.; Al-Youbi, A. O.; Sun, X. Ni_3S_2 Coated ZnO Array for High-Performance Supercapacitors. *J. Power Sources* **2014**, *245*, 463−467.
(25) Pu, Z.; Liu, Q.; H. Qusti, A.; M. Asiri, A.; Al-Youbi, A. O.; Sun, X. Fabrication of $Ni(OH)_2$ Coated ZnO Array for High-Rate Pseudocapacitive Energy Storage. *Electrochim. Acta* **2013**, *109*, 252−255.
(26) Li, G. R.; Wang, Z. L.; Zheng, F. L.; Ou, Y. N.; Tong, Y. X. ZnO@MoO_3 Core/Shell Nanocables: Facile Electrochemical Synthesis and Enhanced Supercapacitor Performances. *J. Mater. Chem.* **2011**, *21*, 4217−4221.
(27) Zhang, G. Q.; Wu, H. B.; Hoster, H. E.; Chan-Park, M. B.; Lou, X. W. Single-Crystalline $NiCo_2O_4$ Nanoneedle Arrays Grown on Conductive Substrates as Binder-free Electrodes for High-Performance Supercapacitors. *Energy Environ. Sci.* **2012**, *5*, 9453−9456.
(28) Jiang, J.; Li, Y.; Liu, J.; Huang, X. Building One-Dimensional Oxide Nanostructure Arrays on Conductive Metal Substrates for Lithium-Ion Battery Anodes. *Nanoscale* **2011**, *3*, 45−58.
(29) Jiang, J.; Li, Y.; Liu, J.; Huang, X.; Yuan, C.; Lou, X. W. Recent Advances in Metal Oxide-based Electrode Architecture Design for Electrochemical Energy Storage. *Adv. Mater.* **2012**, *24*, 5166−5180.
(30) Zhang, G.; Lou, X. W. General Solution Growth of Mesoporous $NiCo_2O_4$ Nanosheets on Various Conductive Substrates as High-Performance Electrodes for Supercapacitors. *Adv. Mater.* **2013**, *25*, 976−979.
(31) Yuan, C.; Yang, L.; Hou, L.; Shen, L.; Zhang, X.; Lou, X. W. Growth of Ultrathin Mesoporous Co_3O_4 Nanosheet Arrays on Ni Foam for High-Performance Electrochemical Capacitors. *Energy Environ. Sci.* **2012**, *5*, 7883−7887.
(32) Wen, Z.; Zhu, L.; Mei, W.; Li, Y.; Hu, L.; Sun, L.; Wan, W.; Ye, Z. A Facile Fluorine-mediated Hydrothermal Route to Controlled Synthesis of Rhombus-shaped Co_3O_4 Nanorod Arrays and Their Application in Gas Sensing. *J. Mater. Chem. A* **2013**, *1*, 7511−7518.
(33) Mei, W.; Huang, J.; Zhu, L.; Ye, Z.; Mai, Y.; Tu, J. Synthesis of Porous Rhombus-shaped Co_3O_4 Nanorod Arrays Grown Directly on a Nickel Substrate with High Electrochemical Performance. *J. Mater. Chem.* **2012**, *22*, 9315−9321.
(34) Saito, N.; Haneda, H.; Seo, W. S.; Koumoto, K. Selective Deposition of ZnF(OH) on Self-Assembled Monolayers in Zn-NH_4F Aqueous Solutions for Micropatterning of Zinc Oxide. *Langmuir* **2001**, *17*, 1461−1469.
(35) Xu, F.; Sun, L.; Dai, M.; Lu, Y. Fluorine-Ion-Mediated Electrodeposition of Rhombus-like ZnFOH Nanorod Arrays: An Intermediate Route to Novel ZnO Nanoarchitectures. *J. Phys. Chem. C* **2010**, *114*, 15377−15382.
(36) Zhu, L.; Wen, Z.; Mei, W.; Li, Y.; Ye, Z. Porous CoO Nanostructure Arrays Converted from Rhombic Co(OH)F and Needle-like $Co(CO_3)_{0.5}(OH)\cdot 0.11H_2O$ and Their Electrochemical Properties. *J. Phys. Chem. C* **2013**, *117*, 20465−20473.
(37) Wang, B.; Zhu, T.; Wu, H. B.; Xu, R.; Chen, J. S.; Lou, X. W. Porous Co_3O_4 Nanowires Derived from Long $Co(CO_3)_{0.5}(OH)\cdot 0.11H_2O$ Nanowires with Improved Supercapacitive Properties. *Nanoscale* **2012**, *4*, 2145−2149.
(38) Liu, X. Y.; Zhang, Y. Q.; Xia, X. H.; Shi, S. J.; Lu, Y.; Wang, X. L.; Gu, C. D.; Tu, J. P. Self-Assembled Porous $NiCo_2O_4$ Hetero-structure Array for Electrochemical Capacitor. *J. Power Sources* **2013**, *239*, 157−163.
(39) Guo, D.; Zhang, H.; Yu, X.; Zhang, M.; Zhang, P.; Li, Q.; Wang, T. Facile Synthesis and Excellent Electrochemical Properties of $CoMoO_4$ Nanoplate Arrays as Supercapacitors. *J. Mater. Chem. A* **2013**, *1*, 7247−7254.
(40) Fan, Z.; Yan, J.; Wei, T.; Zhi, L.; Ning, G.; Li, T.; Wei, F. Asymmetric Supercapacitors Based on Graphene/MnO_2 and Activated Carbon Nanofiber Electrodes with High Power and Energy Density. *Adv. Funct. Mater.* **2011**, *21*, 2366−2375.
(41) Guan, G.; Liu, J.; Cheng, C.; Li, H.; Li, X.; Zhou, W.; Zhang, H.; Fan, H. J. Hybrid Structure of Cobalt Monoxide Nanowire@Nickel Hydroxidenitrate Nanoflake Aligned on Nickel Foam for High-Rate Supercapacitor. *Energy Environ. Sci.* **2011**, *4*, 4496−4499.